


ORIGINAL ARTICLE

Open Access



Indirect Adaptive Robust Trajectory Tracking Control of Hard Rock TBM with Load Variation of Tunneling Face

Chengjun Shao¹, Jianfeng Liao², Zhitao Liu^{1*}  and Hongye Su¹

Abstract

Posture adjustment of open-type hard rock tunnel boring machine (TBM) can be achieved by properly adjusting the hydraulic pressure of gripper cylinder and torque cylinders. However, the time-varying inhomogeneous load acting on tunneling face of TBM and complex stratum working condition can cause the trajectory deviation. In this paper, the position and posture rectification kinematics and dynamics models of TBM have been established in order to track the trajectory. Moreover, there are uncertain parameters and uncertain loads from complex working conditions in the dynamic model. An indirect adaptive robust control strategy is applied to achieve precise position and posture trajectory tracking control. Simulation results show when the position deviation only occurs in *Y*-axis and the current orientation is parallel with the designed axis, the deviation can be corrected by controlling the pressure of gripper cylinder and the actual trajectory meets the designed axis when TBM is pushed forward 0.14 m in *X*-axis. If the deviation only occurs in *Z*-axis, then the deviation can be corrected by controlling torque cylinders. If the position deviation occurs both in *Y*-axis and *Z*-axis at the same time, the pressure of gripper cylinder and torque cylinders should be controlled at the same time to rectify the deviation. Simulation results are shown to illustrate the effectiveness and robustness of the proposed controller. This research proposes an indirect adaptive robust controller that can track the planned tracking trajectory smoothly and rapidly.

Keywords: Open type hard rock TBM, Inhomogeneous load, Position and posture rectification, Indirect adaptive robust control

1 Introduction

Tunnel boring machine (TBM) is a large and complicated special construction equipment for underground tunnel excavation. With the development of national economy construction and infrastructure projects, TBM has been widely used in underground subway constructions, railway or highway tunnels, crossing-river tunnels and national defense constructions in the past decades [1, 2].

Figure 1 shows a diagram of a typical open type hard rock TBM. The open type hard rock TBM contains mainly the cutterhead, driving system, shield, main beam, thrust system, gripper carrier assembly and machine

conveyor. When TBM is working, the rock on the tunnel face is excavated by the cutters installed on the rotating cutterhead driven by the driving system. The thrust force is used to push TBM forward and the gripper shoe works on the surrounding rock tightly to maintain the machine in a constant position. The gripper carrier assembly system shown in Figure 2 includes gripper cylinders and torque cylinders. The position and posture adjustment in horizontal direction of TBM can be achieved by properly adjusting the pressure of gripper cylinder, while the orientation and posture adjustment in vertical direction can be achieved by adjusting the pressure of torque cylinders.

The effect caused by inhomogeneous strong load acting on TBM and complex stratum working condition during the excavation will leads the deviation between practical excavation trajectory and designed trajectory. The constraints such as safety and nonholonomic

*Correspondence: ztliu@zju.edu.cn

¹ State Key Laboratory of Industrial Control Technology, Institute of Cyber-Systems and Control, Zhejiang University, Hangzhou 310027, China

Full list of author information is available at the end of the article

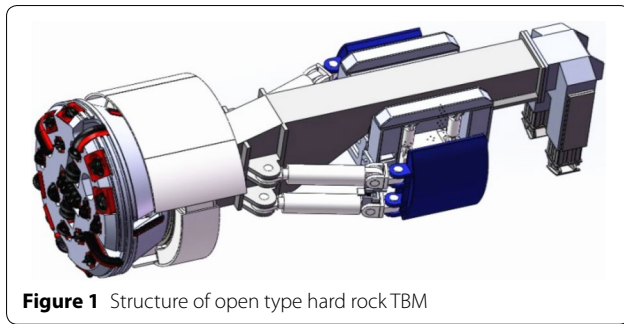


Figure 1 Structure of open type hard rock TBM

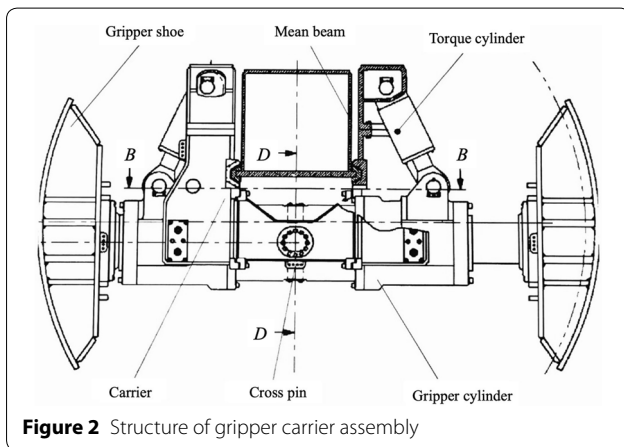


Figure 2 Structure of gripper carrier assembly

constraint are difficult to be completely considered due to the strong coupling among the multi-systems. Manual control method from experienced engineers is the traditional deviation rectification way of TBM, which restricts the development of TBM. So far, there have been some research work about trajectory tracking control for shield machine. Finite element method was applied by Shen et al. to analyze the internal force caused by rolling correction during shield machine tunneling construction [3]. Wang carried out a deep excavation method for shield trajectory rectification under the situation without or with few tiny barriers [4]. For shield machine in a complicated underground environment, an integral sliding mode manifold by replacing the traditional signum with the hyperbolic tangent function was addressed to construct the system controllers to achieve trajectory tracking control in Yue's studies, and numerical simulations were implemented to illustrate the improved performances of the closed-loop system [5]. In addition, Yue et al. [6] proposed a double closed-loop control strategy to tackle the uncertain load acting on shield body and nonlinear factors caused by the hydraulic actuators. Numerical simulations verified the proposed control structure is simple but effective, which yields a potential value for a shield tunneling machine subject to

actuator saturation constraints. Xie et al. [7] discussed the automatic thrust trajectory tracking control of shield tunneling machine under complex stratum working condition. An integrated control system which consists of trajectory generator and individual cylinder controller is proposed to achieve the automatic control of the thrust trajectory. Moreover, a fuzzy PID controller was designed to achieve the orientation and posture adjustment of shield type hard rock TBM by Liu et al. [8]. The current researches focus mainly on shield machine or shield type TBM, which make the position and posture rectification by adjusting the distribution of thrust pressure in corresponding thrust cylinders working zone. However, the mechanical structure of open type hard rock TBM is different from shield machines [9–11]. Gripper carrier assembly is used for deviation rectification of open type TBM rather than thrust system in shield machine.

In this paper, the working mechanism of open type TBM deviation rectification is studied to achieve the trajectory tracking control. The dynamic analysis of cutterhead driving system, main beam, gripper, torque and propel assembly has been established. Inhomogeneous strong load acting on cutterhead and shield is the main factor affect the trajectory deviation. Huo et al. [12–14] carried a dynamic characteristics and structure optimization of TBM cutter system with multi-joint surface. CSM model [15] is applied to describe the interactions between cutterhead and rocks. The mechanism dynamics are deduced from the kinematics using the Lagrange multiplier approach. The established dynamic model is difficult to control, as there exist uncertain parameters and uncertain load, which are caused not only by TBM working in complex stratum conditions, but also by the added difficulties of the coupled complex dynamics of gripper, torque and propel assembly and the extent of unmatched model uncertainties of the combined overall system. The adaptive robust control (ARC) has been validated as an effective control strategy for systems with both uncertain parameters and uncertain nonlinearities [16–19]. ARC effectively integrates adaptive control with robust control though utilizing on-line parameter adaptation to decrease the parametric uncertainties and adopting certain robust control laws to weaken the effects of various uncertainties [20]. However, ARC with discontinuous projection-type parameter estimation algorithm has the drawback that parameter estimates normally do not converge to their true values fast enough as observed in actual use [18, 21]. Then, indirect adaptive robust control (IARC) strategy is proposed in this paper to achieve the precise trajectory tracking control of open type hard rock TBM.

The remaining paper is organized as follows. In Section 2, the dynamic models of open type TBM deviation

rectification system is established. Section 3 gives the proposed indirect adaptive robust controller with proofs of the stability. Section 4 presents the simulation results of the proposed indirect adaptive robust controller and the conclusions are given in Section 5.

2 Dynamic Models of Open Type TBM

The simplified schematics of open type TBM shown in Figure 3 consists of a cutterhead driving system, a mean beam, thrust system and gripper carrier assembly. When the TBM position deviation signal oversteps the allowed scope, horizontal steering will be conducted by adjusting the gripper cylinder and vertical steering will be implemented by manipulating the torque cylinders. Define two frames, reference frame $O_A - x_A y_A z_A$ fixed to the gripper carrier assembly, and the other one, moving frame $O_B - x_B y_B z_B$ attached to the cutterhead at the center. The origin of reference frame is the center of gripper carrier assembly and the origin of moving frame is the center of cutterhead. The posture of open type TBM is defined through the standard Roll-Pitch-Yaw (RPY) angles: first rotate the moving frame around the fixed x -axis by the yaw angle φ , then rotate the moving frame around the fixed y -axis by the pitch angle θ , and finally rotate the moving frame around the fixed z -axis by the roll angle ψ .

Let the generalized coordinate vector of TBM $q = [x_B \ y_B \ z_B \ \varphi \ \theta \ \psi]^T$ which contains position vector $[x_B \ y_B \ z_B]^T$ and posture vector $[\varphi \ \theta \ \psi]^T$. Define ${}^A p_i \in R^3$ as the position vector of a certain point in shield body in reference frame $O_A - x_A y_A z_A$ and ${}^B p_i \in R^3$ as the position vector of a certain point in moving frame $O_B - x_B y_B z_B$. Let ${}^A O_B \in R^3$ be the position vector of the center O_A in frame $O_A - x_A y_A z_A$ and center O_B in frame $O_B - x_B y_B z_B$. Then,

$${}^A p_i = {}^A O_B + {}^A R {}^B p_i, \tag{1}$$

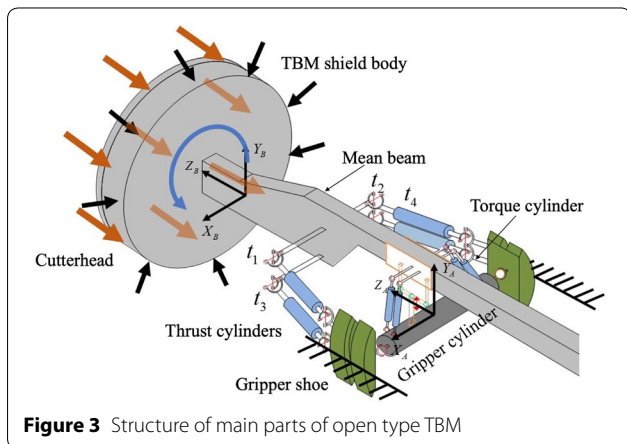


Figure 3 Structure of main parts of open type TBM

where ${}^A_B R$ is the rotational matrix from frame $O_A - x_A y_A z_A$ to frame $O_B - x_B y_B z_B$ and is uniquely determined by posture vector $[\varphi \ \theta \ \psi]^T$, and

$${}^A_B R = \begin{bmatrix} c\psi c\theta & -s\psi c\theta & c\psi s\theta s\varphi & s\psi s\theta c\varphi \\ s\psi c\theta & c\psi c\theta & s\psi s\theta s\varphi & -c\psi s\theta c\varphi \\ -s\theta & c\theta & c\theta s\varphi & c\theta c\varphi \end{bmatrix}, \tag{2}$$

where $c\theta$ and $s\theta$ are short-hand notations for $\cos \theta$ and $\sin \theta$ respectively. ${}^B_A R$ is the orthogonal matrix of ${}^A_B R$:

$${}^B_A R = {}^A_B R^{-1} = {}^A_B R^T. \tag{3}$$

2.1 Kinematics of Open Type TBM

The specific thrust system structure and gripper carrier assembly structure are given in Figures 4 and 5, respectively. And the parallel structures, especially the gripper carrier assembly, are well displayed.

According to the thrust system structure shown in Figure 4, the coordinates of ${}^B t_i$ and ${}^A T_i$ is known in this paper. The length of each thrust cylinder link can be obtained as

$$L_t^i = \left\| {}^A O_B + {}^A_B R {}^B t_i - {}^A T_i \right\| = \left\| {}^A t_i - {}^A T_i \right\| = \left\| {}^A \lambda_{T_i}^{t_i} \right\|, \tag{4}$$

where L_t^i is the length of the i th thrust cylinder link, t_i is the i th joint connecting main beam and thrust rod, T_i is the i th joint connecting gripper shoe and thrust cylinder, ${}^A \lambda_{T_i}^{t_i}$ is the vector from T_i to t_i in reference frame. The unit vector of thrust cylinder can be expressed as

$${}^A e_t^i = \frac{1}{L_t^i} {}^A \lambda_{T_i}^{t_i}. \tag{5}$$

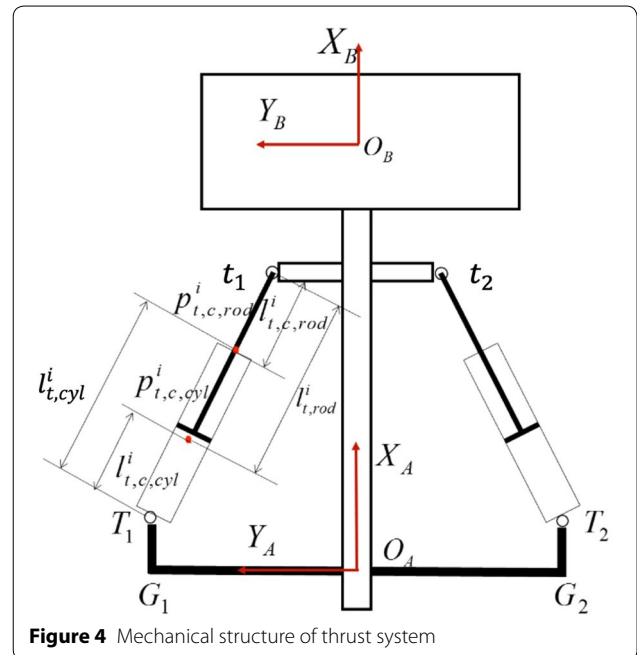


Figure 4 Mechanical structure of thrust system

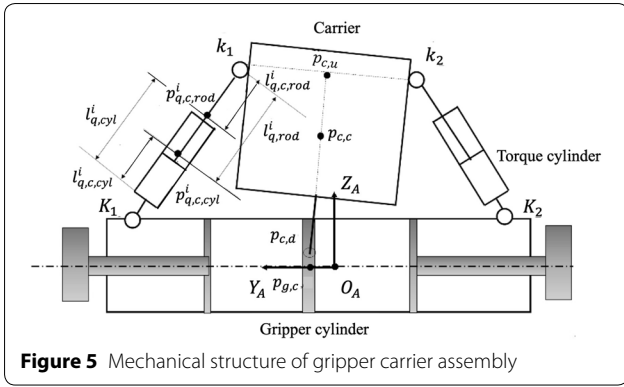


Figure 5 Mechanical structure of gripper carrier assembly

The coordinates of centroid of the i th thrust cylinder ${}^A\mathbf{p}_{t,c,cyl}^i$ and the i th piston rod ${}^A\mathbf{p}_{t,c,rod}^i$ can be defined as

$$\begin{aligned} {}^A\mathbf{p}_{t,c,cyl}^i &= {}^A\mathbf{T}_i + l_{t,c,cyl}^i {}^A\mathbf{e}_t^i, \\ {}^A\mathbf{p}_{t,c,rod}^i &= {}^A\mathbf{t}_i - l_{t,c,rod}^i {}^A\mathbf{e}_t^i, \end{aligned} \quad (6)$$

where $l_{t,c,cyl}^i$ is the distance between centroid of the i th thrust cylinder to joint T_i , $l_{t,c,rod}^i$ is the distance between centroid of the i th thrust cylinder rod to joint t_i .

Referring to Figure 3 and Figure 5, a vector equation is carried out in order to achieve the coordinate of the i th joint connecting carrier and torque cylinder ${}^A\mathbf{k}_i$.

$${}^A\lambda_{O_A}^{p_{g,c}} + {}^A\lambda_{p_{g,c}}^{p_{c,d}} + {}^A\lambda_{p_{c,d}}^{p_{r,d}} + {}^A\lambda_{p_{r,d}}^{O_B} = {}^A\lambda_{O_A}^{O_B}, \quad (7)$$

where $p_{g,c}$ is the centroid of gripper cylinder, $p_{c,d}$ is the joint connecting carrier and gripper, $p_{r,d}$ is a point locating at axis Z_B , ${}^A\lambda_{O_A}^{p_{g,c}} = d_1[0 \ 1 \ 0]^T$, ${}^A\lambda_{p_{g,c}}^{p_{c,d}} = d_2[0 \ 0 \ 1]^T$, d_1 is the displacement of gripper shoe, d_2 is the displacement from $p_{c,d}$ to $p_{g,c}$, ${}^A\lambda_{p_{c,d}}^{p_{r,d}}$ is parallel with the axis X_B , ${}^A\mathbf{O}_B = [x_B \ y_B \ z_B]^T$ is known by laser guidance system. Then, Eq. (7) can be rewritten as

$$\begin{aligned} d_1[0, 1, 0]^T + d_2[0, 0, 1]^T + l_b {}^A R [1, 0, 0]^T \\ = {}^A\mathbf{p}_{r,d} = {}^A\mathbf{O}_B + {}^A\mathbf{R}^B \mathbf{p}_{r,d}, \end{aligned} \quad (8)$$

where ${}^B\mathbf{p}_{r,d} = d_3[0 \ 0 \ 1]^T$ and d_3 is known in this paper. Then, d_1 , d_2 and l_b can be calculated by

$$\begin{aligned} l_b &= \frac{x_B}{\cos \varphi \cos \theta}, \\ d_1 &= y_B - x_B \tan \psi, \\ d_2 &= z_B + \frac{x_B}{\cos \psi} \tan \theta. \end{aligned} \quad (9)$$

The centroid of the i th gripper cylinder ${}^A\mathbf{p}_{g,c}^i$ and the i th connecting joint of the carrier and gripper cylinder ${}^A\mathbf{p}_{c,d}^i$ can be expressed as

$$\begin{aligned} {}^A\mathbf{p}_{g,c} &= [0 \ d_1 \ 0]^T, \\ {}^A\mathbf{p}_{c,d} &= [0 \ d_1 \ d_2]^T. \end{aligned} \quad (10)$$

Then, the coordinate of ${}^A\mathbf{k}_i$ can be expressed as

$${}^A\mathbf{k}_i = {}^A\mathbf{p}_{c,d} + {}^A\mathbf{R}^B \lambda_{p_{c,d}}^{k_i}. \quad (11)$$

And the centroid of torque cylinder and cylinder rod can be obtained as

$$\begin{aligned} {}^A\mathbf{p}_{q,c,cyl}^i &= {}^A\mathbf{K}_i + l_{q,c,cyl}^i {}^A\mathbf{e}_q^i, \\ {}^A\mathbf{p}_{q,c,rod}^i &= {}^A\mathbf{k}_i + l_{q,c,rod}^i {}^A\mathbf{e}_q^i, \end{aligned} \quad (12)$$

where K_i is the i th joint connecting gripper cylinder and torque cylinder, $l_{q,c,cyl}^i$ is the distance from centroid of torque cylinder to joint K_i , $l_{q,c,rod}^i$ is the distance from centroid of torque cylinder rod to joint k_i , ${}^A\mathbf{e}_q^i = ({}^A\mathbf{k}_i - {}^A\mathbf{K}_i) / l_{q,c,rod}^i$.

2.1.1 Kinematics of Thrust System

The angular velocity of open type TBM shield body in reference frame and moving frame can be obtained as follows:

$$\begin{aligned} {}^A\boldsymbol{\omega}_r &= {}^A\mathbf{J}_\omega^p \dot{\mathbf{q}}, \\ {}^B\boldsymbol{\omega}_r &= {}^B\mathbf{J}_\omega^p \dot{\mathbf{q}}, \end{aligned} \quad (13)$$

where ${}^A\mathbf{J}_\omega^p = [0_{3 \times 3} \ {}^A\boldsymbol{\Omega}_r]$, ${}^A\boldsymbol{\Omega}_r = \begin{bmatrix} c\theta c\psi & -s\psi & 0 \\ c\theta s\psi & c\psi & 0 \\ -s\theta & 0 & 1 \end{bmatrix}$,

$${}^B\mathbf{J}_\omega^p = [0_{3 \times 3} \ {}^B\boldsymbol{\Omega}_r], \quad {}^B\boldsymbol{\Omega}_r = \begin{bmatrix} 1 & 0 & -s\theta \\ 0 & c\varphi & s\varphi c\theta \\ 0 & -s\varphi & c\varphi c\theta \end{bmatrix}.$$

The velocity of centroid of the TBM shield body in reference frame can be described as

$${}^A\dot{\mathbf{p}}_{r,c} = {}^A\dot{\mathbf{O}}_B + {}^A\boldsymbol{\omega}_r \times {}^B\mathbf{p}_{r,c} = {}^A\mathbf{J}_v^{p_{r,c}} \dot{\mathbf{q}}, \quad (14)$$

where $p_{r,c}$ is the centroid of TBM shield body, ${}^A\mathbf{J}_v^{p_{r,c}} = [E_{3 \times 3} \ -S({}^B\mathbf{p}_{r,c})^A\boldsymbol{\Omega}_r]$.

Define a symmetric matrix

$$S(\mathbf{u}) = \begin{bmatrix} 0 & -u_z & u_y \\ u_z & 0 & -u_x \\ -u_y & u_x & 0 \end{bmatrix},$$

where $\mathbf{u} = [u_x \ u_y \ u_z]^T$.

The velocity of the i th joint t_i can be written as

$${}^A\dot{\mathbf{t}}_i = {}^A\dot{\mathbf{O}}_B + {}^A\boldsymbol{\omega}_r \times {}^B\mathbf{t}_i = {}^A\mathbf{J}_v^{t_i} \dot{\mathbf{q}}, \quad (15)$$

where ${}^A\mathbf{J}_v^{t_i} = [E_{3 \times 3} \ -S({}^B\mathbf{t}_i)^A\boldsymbol{\Omega}_r]$.

The velocity of the i th joint t_i can be rewritten as below based on the principle of kinematic synthesis:

$${}^A\dot{\mathbf{t}}_i = \dot{l}_t^i {}^A\mathbf{e}_t^i + l_t^i {}^A\boldsymbol{\omega}_t^i \times {}^A\mathbf{e}_t^i. \quad (16)$$

Combining Eqs. (15), (16), the extension velocity of the i th thrust cylinder can be obtained as

$${}^A \dot{L}_t^i = {}^A \dot{t}_i \cdot {}^A e_t^i = {}^A J_s^{t_i} \dot{q}, \quad (17)$$

where ${}^A J_s^{t_i} = {}^A e_t^{iT} {}^A J_v^{t_i}$.

The characteristics of universal joints connecting thrust cylinders and gripper shoes are taken into consideration to obtain the angular velocity of thrust cylinders and rods. The structure of universal joint is presented in Figure 6.

According to Harib's method [22], the angular velocity of the i th thrust cylinder can be described as

$${}^A \omega_i = {}^A \omega_u^i {}^A u_i + {}^A \omega_v^i {}^A v_i = {}^A J_{\omega,t}^i \dot{q}, \quad (18)$$

where

$${}^A J_{\omega,t}^i = \frac{1}{L_t^i {}^A e_t^i \cdot {}^A n_i} (-{}^A u_i {}^A v_i^T + {}^A v_i {}^A u_i^T) ({}^A J_v^{t_i} - {}^A e_t^i {}^A J_s^{t_i}),$$

$${}^A u_i = [0 \ 0 \ 1]^T, \quad {}^A v_i = \frac{{}^A u_i \times {}^A e_t^i}{\|{}^A u_i \times {}^A e_t^i\|}, \quad {}^A n_i = {}^A u_i \times {}^A v_i.$$

The angular velocity of thrust cylinders and rods in moving frame can be expressed as

$${}^B \omega_t^i = {}^B \Omega_t^{iA} \Omega_t^{i-1A} \omega_t^i = {}^B J_{\omega,t}^i \dot{q}, \quad (19)$$

where ${}^B J_{\omega,t}^i = {}^B \Omega_t^{iA} \Omega_t^{i-1A} {}^A J_{\omega,t}^i$.

Then the centroid velocity of the i th thrust cylinder is

$${}^A \dot{p}_{t,c,cyl}^i = l_{t,c,cyl}^i {}^A \omega_t^i \times {}^A e_t^i = {}^A J_v^{p_{t,c,cyl}^i} \dot{q}, \quad (20)$$

where ${}^A J_v^{p_{t,c,cyl}^i} = -l_{t,c,cyl}^i S({}^A e_t^i) {}^A J_{\omega,t}^i$.

And the centroid velocity of the i th thrust cylinder rod is

$${}^A \dot{p}_{t,c,rod}^i = {}^A \dot{t}_i - l_{t,c,rod}^i {}^A \omega_t^i \times {}^A e_t^i = {}^A J_v^{p_{t,c,rod}^i} \dot{q}, \quad (21)$$

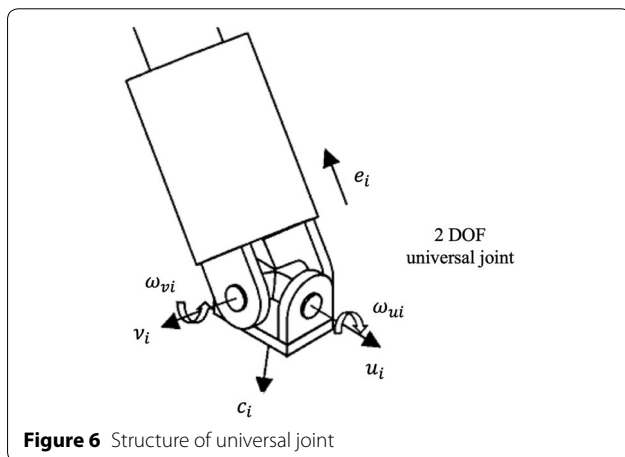


Figure 6 Structure of universal joint

where ${}^A J_v^{p_{t,c,rod}^i} = {}^A J_v^{t_i} + l_{t,c,rod}^i S({}^A e_t^i) {}^A J_{\omega,t}^i$.

2.1.2 Kinematics of TBM Gripper Carrier Assembly

Differentiating Eq. (10), the velocity of gripper cylinder ${}^A \dot{p}_{g,c}$ and connecting joint of carrier and gripper cylinder ${}^A \dot{p}_{c,d}$ can be written as,

$$\begin{aligned} {}^A \dot{p}_{g,c} &= {}^A J_v^g \dot{q}, \\ {}^A \dot{p}_{c,d} &= {}^A J_v^{p_{c,d}} \dot{q}. \end{aligned} \quad (22)$$

The velocity of centroid of carrier is

$${}^A \dot{p}_{c,c} = {}^A \dot{p}_{c,d} + {}^A \omega_r \times {}^A \lambda_{p_{c,c}}^{p_{c,d}} = {}^A J_v^{p_{c,c}} \dot{q}, \quad (23)$$

where ${}^A J_v^{p_{c,c}} = {}^A J_v^{p_{c,d}} \dot{q} - [0_{3 \times 3}, S({}^A \lambda_{p_{c,d}}^{p_{c,c}}) {}^A \Omega_r]$.

The velocity of the i th joint ${}^A k_i$ is

$${}^A \dot{k}_i = {}^A \dot{p}_{c,d} + {}^A \omega_r \lambda_{p_{c,d}}^{k_i} = {}^A J_v^{k_i} \dot{q}, \quad (24)$$

where ${}^A J_v^{k_i} = {}^A J_v^{p_{c,d}} - [0_{3 \times 3}, S({}^A \lambda_{p_{c,d}}^{k_i}) {}^A \Omega_r]$.

According to Eq. (16), ${}^A k_i$ can be rewritten as

$${}^A \dot{k}_i = {}^A \dot{K}_i + L_q^i {}^A \omega_q^i \times {}^A e_q^i + \dot{L}_q^i {}^A e_q^i. \quad (25)$$

Then, the extension velocity and angular velocity of torque cylinder can be obtained as

$$\dot{L}_q^i = ({}^A \dot{k}_i - {}^A \dot{K}_i) \cdot {}^A e_q^i = {}^A J_s^{k_i} \dot{q}, \quad (26)$$

$${}^A \omega_q^i = \frac{{}^A e_q^i \times ({}^A k_i - {}^A K_i)}{L_q^i} + \dot{\phi}_x^i {}^A e_q^i = {}^A J_{\omega}^{k_i} \dot{q}, \quad (27)$$

where ${}^A J_s^{k_i} = {}^A e_q^{iT} ({}^A J_v^{k_i} - {}^A J_v^g)$, $\dot{\phi}_x^i$ is the self-rotating angular velocity of torque cylinder. In this paper, the influence of self-rotation is small enough to be ignored, so

$${}^A J_{\omega}^{k_i} = \frac{1}{L_q^i} S({}^A e_q^i) ({}^A J_v^{k_i} - {}^A J_v^g), \quad (28)$$

$${}^B \omega_q^i = {}^B \Omega_q^{iA} \Omega_q^{i-1A} \omega_q^i = {}^B J_{\omega,q}^i \dot{q},$$

where ${}^B J_{\omega,q}^i = {}^B \Omega_q^{iA} \Omega_q^{i-1A} {}^A J_{\omega,q}^i$.

The velocity of centroid of torque cylinder and rod can be described as

$$\begin{aligned} {}^A \dot{p}_{q,c,cyl}^i &= {}^A \dot{K}_i + l_{q,c,cyl}^i {}^A \omega_q^i \times {}^A e_q^i = {}^A J_v^{p_{q,c,cyl}^i} \dot{q}, \\ {}^A \dot{p}_{q,c,rod}^i &= {}^A \dot{k}_i + l_{q,c,rod}^i {}^A \omega_q^i \times {}^A e_q^i = {}^A J_v^{p_{q,c,rod}^i} \dot{q}, \end{aligned} \quad (29)$$

where $AJ_v^{p_{q,c,cyl}^i} = AJ_v^g - J_{q,c,cyl}^i S(Ae_q^i) AJ_{\omega,q}^i$ and $AJ_v^{p_{q,c,rod}^i} = AJ_v^k + J_{q,c,rod}^i S(Ae_q^i) AJ_{\omega,q}^i$

2.2 Generalized Force of Coupled Multi-Systems

Virtual work principle [23] is applied to derive the expressions of generalize forces acting on the open type TBM. According to Eq. (17), the virtue work of thrust system can be calculated as

$$\delta W_{tsys} = \sum_{i=1}^4 A F_t^i \delta L_t^i = \sum_{i=1}^4 F_t^{iTA} J_s^{ti} \delta q = \tau_t^T \delta q, \quad (30)$$

where $A\tau_t = \sum_{i=1}^4 AJ_s^{tiT} F_t^i = \sum_{i=1}^4 AJ_s^{tiT} (S_{t,A}^i P_{t,A}^i - S_{t,B}^i P_{t,B}^i - b_t^i \dot{L}_t^i) = B_t P_t - C_t \dot{q}$ is the generalized force of thrust system. $S_{t,A}^i$ and $S_{t,B}^i$ are the inlet and outlet cross section area of the i th thrust cylinder, $P_{t,A}^i$ and $P_{t,B}^i$ are the inlet and outlet hydraulic pressure of the i th thrust cylinder, b_t^i is the damping coefficient.

Then, the generalized force of gripper carrier assembly can be obtained similarly as

$$A\tau_c = AJ_s^{gTA} F_g + \sum_{i=1}^4 AJ_s^{kiT} F_q^i - \sum_{i=1}^4 F_q^{iA} e_q^{iTA} J_v^g, \quad (31)$$

where $F_g = p_g^i S_{g,A} - p_g^i S_{g,B} - b_g \dot{L}_g$ is the generalized force of gripper cylinder, $F_q^i = p_{q,A}^i S_{q,A} - p_{q,B}^i S_{q,B} - b_q^i \dot{L}_q^i$ is the generalized force of the i th torque cylinder.

As mentioned before, the effect caused by inhomogeneous strong load acting on TBM is one of the main factors leading to the trajectory deviation. It's necessary to establish the model of generalized force acting on cutterhead and front shield, and CSM model is adopted in this paper. Figure 7 shows the principle of disc cutting the rock, the formula to estimate the generalized force acting on cutterhead is as follows.

The force of the i th single disc cutter is

$$F_{rock}^i = \frac{C^3 \sqrt{\frac{s}{\Phi \sqrt{RT}} \sigma_c^2 \sigma_t \Phi RT}}{1 + \Psi}, \quad (32)$$

where C is a dimensionless parameter, s is the area between the disc cutters, R is the radius of disc cutter, $\Phi = \arccos((R - p_h)/R)$ is the angle between disc cutter and rock, T is the tip width of disc cutter, p_h is penetration, Ψ is a constant of the pressure distribution function, σ_t is the tensile strength of rock, σ_c is the uniaxial compressive strength (UCS) of rock.

The normal force and tangential force of the i th single disc cutter can be expressed as

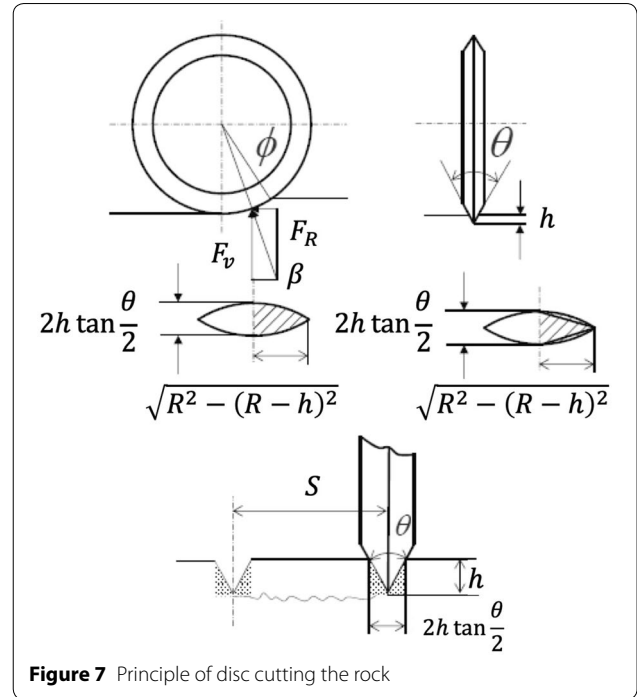


Figure 7 Principle of disc cutting the rock

$$\begin{aligned} F_{rock,n}^i &= F_{rock}^i \cos(\Phi/2), \\ F_{rock,t}^i &= F_{rock}^i \sin(\Phi/2). \end{aligned} \quad (33)$$

According to Eqs. (32) and (33), the generalized force of single disc cutter acting on cutterhead in moving frame can be described as

$$\begin{aligned} {}^B F_{rock}^i &= [-F_{rock,n}^i, F_{rock,t}^i s(\gamma_i) \text{sgn}(\omega), \\ &\quad -F_{rock,t}^i c(\gamma_i) \text{sgn}(\omega)]^T, \end{aligned} \quad (34)$$

where γ_i is rotation angle of cutterhead.

The point of force application of the i th disc cutter can be determined as

$${}^B r_i = [d, r_i \cos(\gamma_i), r_i \sin(\gamma_i)]^T. \quad (35)$$

The equivalent torque of the i th disc cutter acting on cutterhead can be written as

$${}^B T_{rock}^i = \text{cross}({}^B r_i, {}^B F_{rock}^i). \quad (36)$$

The load of main driving system is not included in the torque acting on TBM caused by surrounding rock through driving system, then

$${}^B T_{rock,d}^i = \text{diag}(1, 1, 1, 1, 0) {}^B T_{rock}^i. \quad (37)$$

Let T_e be the torque acting on the cutterhead by main driving system, then the torque acting on TBM can be expressed as

$${}^B T_{rock,r}^i = {}^B T_{rock,d}^i + [0, 0, 0, 0, 0, 1]^T T_e. \quad (38)$$

The generalized force caused by surrounding rock can be described as

$${}^A \tau_{rock} = \sum_{i=1}^n {}^A {}_B R [{}^B F_{rock}^i, {}^B T_{rock,r}^i]^T. \quad (39)$$

The friction force between TBM and surrounding rock is highly complex, some simplifications have been taken in this paper. Assume the friction force can be divided into slide friction force, pitch friction force, roll friction force, yaw friction force, and each of them are independent. The reset integrator friction model is used to describe the complex model.

$$\frac{dz}{dt} = \begin{cases} 0, & \text{if } (v > 0 \text{ and } z \geq z_0) \text{ or } (v < 0 \text{ and } z \leq -z_0), \\ v, & \text{otherwise,} \end{cases} \quad (40)$$

where z is relatively displacement of two surfaces, v is the velocity of TBM.

The slide friction force can be obtained as

$$F_s = (1 + a(z_s))(\lambda_1 \mu_d^s + \lambda_2 \mu_d^s) z_s + \sigma_1^s \frac{dz_s}{dt}, \quad (41)$$

$${}^B F_s = [-1, 0, 0, 0, 0]^T F_s = C_{nd}^s \lambda + \tau_{fv}^s,$$

where $\sigma_1 dz/dt$ is a damping term, μ_d is friction coefficient, $C_{nd}^s = [-1, 0, 0, 0, 0]^T (1 + a(z_s)) z_s [\mu_d^s, \mu_d^s]$, $\tau_{fv}^s = \sigma_1^s dz_r/dt$, $a(z)$ is a viscous effect function:

$$a(z) = \begin{cases} a, & \text{if } |z| < z_0, \\ 0, & \text{otherwise.} \end{cases} \quad (42)$$

The pitch friction force can be written as

$$F_p = (1 + a(z_p))(\lambda_1 \mu_d^p + \lambda_2 \mu_d^p) z_p + \sigma_1^p \frac{dz_p}{dt}, \quad (43)$$

$${}^B F_p = [0, 0, 0, 0, -1, 0]^T F_p = C_{nd}^p \lambda + \tau_{fv}^p,$$

where $C_{nd}^p = [0, 0, 0, 0, 0, -1]^T (1 + a(z_p)) z_p [\mu_d^p, \mu_d^p]$, $\tau_{fv}^p = \sigma_1^p dz_p/dt$.

The roll friction force can be written as

$$F_r = (1 + a(z_r))(\lambda_1 \mu_d^r + \lambda_2 \mu_d^r) z_r + \sigma_1^r \frac{dz_r}{dt}, \quad (44)$$

$${}^B F_r = [0, 0, 0, 0, -1, 0]^T F_r = C_{nd}^r \lambda + \tau_{fv}^r,$$

where $C_{nd}^r = [0, 0, 0, 0, 0, -1]^T (1 + a(z_r)) z_r [\mu_d^r, \mu_d^r]$, $\tau_{fv}^r = \sigma_1^r dz_r/dt$.

The yaw friction force can be written as

$$F_y = (1 + a(z_y))(\lambda_1 \mu_d^y + \lambda_2 \mu_d^y) z_y + \sigma_1^y \frac{dz_y}{dt}, \quad (45)$$

$${}^B F_y = [0, 0, 0, 0, -1, 0]^T F_y = C_{nd}^y \lambda + \tau_{fv}^y,$$

where $C_{nd}^y = [0, 0, 0, 0, 0, -1]^T (1 + a(z_y)) z_y [\mu_d^y, \mu_d^y]$, $\tau_{fv}^y = \sigma_1^y dz_y/dt$.

The generalized friction force in reference frame can be described as

$${}^A \tau_f = \begin{bmatrix} {}^A R & \mathbf{0} \\ \mathbf{0} & {}^A R \end{bmatrix} ({}^B F_s + {}^B F_r + {}^B F_p + {}^B F_y) = C_{nd} \lambda + \tau_{fv}, \quad (46)$$

where $C_{nd} = \begin{bmatrix} {}^A R & \mathbf{0} \\ \mathbf{0} & {}^A R \end{bmatrix} (C_{nd}^s + C_{nd}^r + C_{nd}^p + C_{nd}^y)$, $\tau_{fv} = \tau_{fv}^s + \tau_{fv}^r + \tau_{fv}^p + \tau_{fv}^y$.

Overall, the total generalized force acting on TBM can be obtained as

$${}^A \tau = {}^A \tau_t + {}^A \tau_c + {}^A \tau_{rock} + {}^A \tau_f. \quad (47)$$

In this paper, the gripper cylinder and torque cylinders are the actuators to correct the deviations. Hydraulic pressure of gripper cylinder and torque cylinders are treated as the control vector u , the expression of Eq. (31) can be rewritten as

$$\tau_c = B_c u - C_c \dot{q}. \quad (48)$$

Substituting the expressions into Eq. (47), the total generalized force can be rewritten as

$${}^A \tau = B_c u - (C_c + C_t) \dot{q} + B_t P_t + {}^A \tau_{rock} + {}^A \tau_f. \quad (49)$$

2.3 Dynamic Modelling of Coupled Multi-Systems

Lagrange method is utilized to achieve the dynamic model, the expressions of kinetic energy of TBM shield beam assembly, thrust system and gripper carrier assembly are as follows respectively

$$K_r = \frac{1}{2} \dot{q}^T M_r \dot{q},$$

$$K_{tsys} = \frac{1}{2} \dot{q}^T M_{tsys} \dot{q}, \quad (50)$$

$$K_{csys} = \frac{1}{2} \dot{q}^T M_{csys} \dot{q},$$

where $M_r = m_r {}^A J_v^{pr,cT} A J_v^{pr,c} + B J_\omega^T I_r B J_\omega^r$,

$$\begin{aligned}
 \mathbf{M}_{tsys} &= \sum_{i=1}^4 ({}^A\mathbf{J}_v^{p_{t,c,cyl}^i} \mathbf{m}_{t,cyl}^i {}^A\mathbf{J}_v^{p_{t,c,cyl}^i} + {}^B\mathbf{J}_{\omega,t,cyl}^i \mathbf{I}_{t,cyl}^i {}^B\mathbf{J}_{\omega,t,cyl}^i \\
 &\quad + {}^A\mathbf{J}_v^{p_{t,c,rod}^i} \mathbf{m}_{t,rod}^i {}^A\mathbf{J}_v^{p_{t,c,rod}^i} + {}^B\mathbf{J}_{\omega,t,rod}^i \mathbf{I}_{t,rod}^i {}^B\mathbf{J}_{\omega,t,rod}^i), \\
 \mathbf{M}_{csys} &= \sum_{i=1}^4 ({}^A\mathbf{J}_v^{p_{q,c,cyl}^i} \mathbf{m}_{q,cyl}^i {}^A\mathbf{J}_v^{p_{q,c,cyl}^i} + {}^B\mathbf{J}_{\omega,q}^i \mathbf{I}_{q,cyl}^i {}^B\mathbf{J}_{\omega,q}^i \\
 &\quad + {}^A\mathbf{J}_v^{p_{q,c,rod}^i} \mathbf{m}_{q,rod}^i {}^A\mathbf{J}_v^{p_{q,c,rod}^i} + {}^B\mathbf{J}_{\omega,q}^i \mathbf{I}_{q,rod}^i {}^B\mathbf{J}_{\omega,q}^i) \\
 &\quad + {}^A\mathbf{J}_v^{p_{c,c}^i} \mathbf{m}_c^i {}^A\mathbf{J}_v^{p_{c,c}^i} + {}^A\mathbf{J}_v^{g^i} \mathbf{m}_g^i {}^A\mathbf{J}_v^{g^i} + {}^B\mathbf{J}_{\omega,r}^i \mathbf{I}_c^i {}^B\mathbf{J}_{\omega,r}^i.
 \end{aligned}$$

$$\frac{\partial \mathbf{M}^T}{\partial \mathbf{q}} = \left[\frac{\partial \mathbf{M}}{\partial q_1}, \frac{\partial \mathbf{M}}{\partial q_2}, \dots, \frac{\partial \mathbf{M}}{\partial q_6} \right]^T \in R^{36 \times 6},$$

$$\mathbf{I}_6 \otimes \dot{\mathbf{q}}^T = \begin{bmatrix} \dot{q}^T & & & & & \\ & \dot{q}^T & & & & \\ & & \dot{q}^T & & & \\ & & & \dot{q}^T & & \\ & & & & \dot{q}^T & \\ & & & & & \dot{q}^T \end{bmatrix} \in R^{6 \times 36}.$$

The potential energy can be expressed as follows:

$$\begin{aligned}
 V_r &= m_r g z_{r,c}, \\
 V_{tsys} &= \sum_{i=1}^4 (m_{t,cyl}^i g z_{t,c,cyl}^i + m_{t,rod}^i g z_{t,c,rod}^i), \\
 V_{csys} &= m_c g z_{c,c} + \sum_{i=1}^4 (m_{q,cyl}^i g z_{q,c,cyl}^i + m_{q,rod}^i g z_{q,c,rod}^i).
 \end{aligned} \tag{51}$$

The Lagrangian function is given as

$$L(\mathbf{q}, \dot{\mathbf{q}}) = K(\mathbf{q}, \dot{\mathbf{q}}) - V(\mathbf{q}), \tag{52}$$

where $K(\mathbf{q}, \dot{\mathbf{q}}) = K_r + K_{tsys} + K_{csys}$,

$$V(\mathbf{q}) = V_r + V_{tsys} + V_{csys}.$$

The Euler–Lagrange equation is obtained as

$$\frac{d}{dt} \frac{\partial L}{\partial \dot{\mathbf{q}}} - \frac{\partial L}{\partial \mathbf{q}} = \boldsymbol{\tau}. \tag{53}$$

According to Eqs. (52) and (53), the dynamic model can be expressed as

$$\mathbf{M}(\mathbf{q})\ddot{\mathbf{q}} + \mathbf{C}(\mathbf{q}, \dot{\mathbf{q}})\dot{\mathbf{q}} + \mathbf{G}(\mathbf{q}) = \boldsymbol{\tau} + \boldsymbol{\tau}_d. \tag{54}$$

Substituting Eq. (49) into Eq. (54), the dynamic model can be rewritten as

$$\begin{aligned}
 &\mathbf{M}(\mathbf{q})\ddot{\mathbf{q}} + \mathbf{C}(\mathbf{q}, \dot{\mathbf{q}})\dot{\mathbf{q}} + \mathbf{G}(\mathbf{q}) \\
 &= \mathbf{B}_c \mathbf{u} - (\mathbf{C}_c + \mathbf{C}_t)\dot{\mathbf{q}} + \mathbf{B}_t \mathbf{P}_t + \boldsymbol{\tau}_{rock} + \boldsymbol{\tau}_f + \boldsymbol{\tau}_d, \\
 &\ddot{\mathbf{q}} = \mathbf{M}^{-1}(\mathbf{q})[-\mathbf{C}_h \dot{\mathbf{q}} + \mathbf{G}(\mathbf{q}) + \mathbf{B}_c \mathbf{u} + \mathbf{B}_t \mathbf{P}_t + \boldsymbol{\tau}_{rock} + \boldsymbol{\tau}_f + \boldsymbol{\tau}_d],
 \end{aligned} \tag{55}$$

where $\mathbf{M}(\mathbf{q}) = \mathbf{M}_r + \mathbf{M}_{tsys} + \mathbf{M}_{csys}$ is a mass matrix, $\mathbf{G}(\mathbf{q}) = \partial V / \partial \mathbf{q} = [\partial V / \partial q_1, \partial V / \partial q_2, \dots, \partial V / \partial q_6]^T$ is the gravity term, $\boldsymbol{\tau}_d$ is the bounded unknown disturbances including unstructured dynamics, \mathbf{P}_t is the hydraulic pressure vector of thrust cylinders, $\mathbf{C}_h = \mathbf{C}(\mathbf{q}, \dot{\mathbf{q}}) + \mathbf{C}_c + \mathbf{C}_t$, $\mathbf{C}(\mathbf{q}, \dot{\mathbf{q}})$ is the Coriolis and centrifugal terms

$$\mathbf{C}(\mathbf{q}, \dot{\mathbf{q}}) = \frac{1}{2} [\dot{\mathbf{M}}(\mathbf{q}) + \mathbf{U}_m^T - \mathbf{U}_m], \quad \mathbf{U}_m = (\mathbf{I}_6 \otimes \dot{\mathbf{q}}^T) \frac{\partial \mathbf{M}^T}{\partial \mathbf{q}},$$

Define a set of state variables $\mathbf{x} = [\mathbf{x}_1^T \ \mathbf{x}_2^T]^T = [\mathbf{q}^T \ \dot{\mathbf{q}}^T]^T$. Then the entire system can be expressed in a state-space form as

$$\begin{cases} \dot{\mathbf{x}}_1 = \mathbf{x}_2, \\ \dot{\mathbf{x}}_2 = \mathbf{M}^{-1}(\mathbf{x}_1)[-C_h \mathbf{x}_2 + \mathbf{G}(\mathbf{x}_1) + \mathbf{B}_c \mathbf{u} + \mathbf{B}_t \mathbf{P}_t + \boldsymbol{\tau}_c], \end{cases} \tag{56}$$

where $\boldsymbol{\tau}_c = \boldsymbol{\tau}_{rock} + \boldsymbol{\tau}_f + \boldsymbol{\tau}_d$.

3 Indirect Adaptive Robust Controller

According to Eq. (56), there are unknown parameters such as \mathbf{C}_h and $\mathbf{G}(\mathbf{x}_1)$, and uncertain load represented by $\boldsymbol{\tau}_c$ in the entire coupling multi-system. The proposed IARC strategy can deal effectively with the parametric uncertainties and uncertain nonlinearities.

Define a switching-function-like quantity \mathbf{z}_2 as

$$\mathbf{z}_2 = \dot{\mathbf{z}}_1 + \mathbf{K}_c \mathbf{z}_1, \tag{57}$$

where $\mathbf{z}_1 = \mathbf{x}_1 - \mathbf{y}_d$ is the trajectory tracking error vector and \mathbf{K}_c is a positive definite diagonal feedback matrix, \mathbf{y}_d is the planned tracking trajectory. If \mathbf{z}_2 converge to a small value or zero, then the tracking error \mathbf{z}_1 will converge to a small value or zero, since the transfer function $G(s) = z_1(s)/z_2(s) = 1/(s + K_c)$ is stable. Then, the next objective is to design the hydraulic pressure \mathbf{u} to make \mathbf{z}_2 as small as possible.

Define the unknown parameter vector in state-space as $\boldsymbol{\beta}_t = [C_{h1}, \dots, C_{h6}, \tau_{t1}, \dots, \tau_{t6}]^T$. Let $\hat{\boldsymbol{\beta}}$ denote the estimate of $\boldsymbol{\beta}$ and $\tilde{\boldsymbol{\beta}} = \hat{\boldsymbol{\beta}} - \boldsymbol{\beta}$ is the estimation error. The unknown parameters can be rewritten as

$$-\tilde{\mathbf{C}}_h \mathbf{x}_2 + \tilde{\boldsymbol{\tau}}_t = \boldsymbol{\varphi}^T(\mathbf{x}_1, \mathbf{x}_2) \tilde{\boldsymbol{\beta}}_t, \tag{58}$$

where $\boldsymbol{\varphi} = [-\text{diag}(\mathbf{x}_2), \mathbf{E}_{6 \times 6}]^T$ is a regressor.

The desired hydraulic pressure \mathbf{u} of gripper cylinder and torque cylinders consists of two terms

$$\mathbf{u}_d = \mathbf{u}_{da} + \mathbf{u}_{ds}, \tag{59}$$

where \mathbf{u}_{da} represents the adjustable model compensation needed for perfect tracking in the absence of uncertain nonlinearities

$$\mathbf{u}_{da} = \mathbf{B}_c^{-1} \mathbf{M}(\ddot{\mathbf{y}}_d - \mathbf{K}_c \dot{\mathbf{z}}_1) - \boldsymbol{\varphi}_2^T \hat{\boldsymbol{\beta}}_t. \quad (60)$$

And \mathbf{u}_{ds} is a robust control law consists of two terms:

$$\begin{aligned} \mathbf{u}_{ds} &= \mathbf{u}_{ds1} + \mathbf{u}_{ds2}, \\ \mathbf{u}_{ds1} &= -\mathbf{B}_c^{-1} \mathbf{M} \mathbf{K}_2 \mathbf{z}_2, \end{aligned} \quad (61)$$

where \mathbf{K}_2 is a positive definite feedback gain matrix, \mathbf{u}_{ds1} is a simple proportional feedback to stabilize the nominal system and \mathbf{u}_{ds2} is synthesized to dominate the model uncertainties which is chosen to satisfy the following conditions:

$$\begin{cases} \mathbf{z}_2^T \mathbf{M}^{-1} (\mathbf{B}_c \mathbf{u}_{ds2} - \boldsymbol{\varphi}^T \tilde{\boldsymbol{\beta}}) \leq \varepsilon, \\ \mathbf{z}_2^T \mathbf{M}^{-1} \mathbf{B}_c \mathbf{u}_{ds2} \leq 0, \end{cases} \quad (62)$$

where ε is a positive design parameter that can be arbitrarily small. The first condition preserves the stabilizing characteristics of the robust feedback and the second represents the approximation accuracy requirement. How to choose \mathbf{u}_{ds2} to satisfy the constraints like Eq. (62) can be found in Yao's research [19].

In order to obtain the adaptive robust control law, the estimated unknown parameter vector $\hat{\boldsymbol{\beta}}$ should be calculated. The discontinuous projection parameter adaptation method showing below has been used in subsequent ARC designs and applications [24, 25].

$$\dot{\hat{\boldsymbol{\beta}}} = \text{Proj}_{\hat{\boldsymbol{\beta}}}(\boldsymbol{\Gamma} \boldsymbol{\sigma}), \quad \hat{\boldsymbol{\beta}}(0) \in \Omega_{\boldsymbol{\beta}}, \quad (63)$$

$$\text{Proj}_{\hat{\boldsymbol{\beta}}}(\cdot)_i = \begin{cases} 0, & \text{if } \hat{\boldsymbol{\beta}}_i = \boldsymbol{\beta}_{i\max} \text{ and } \cdot_i > 0, \\ 0, & \text{if } \hat{\boldsymbol{\beta}}_i = \boldsymbol{\beta}_{i\min} \text{ and } \cdot_i < 0, \\ \cdot_i, & \text{otherwise,} \end{cases} \quad (64)$$

where $\boldsymbol{\Gamma}$ is a positive definite diagonal matrix of adaptation rates and $\boldsymbol{\sigma}$ is a parameter adaptation function, $\boldsymbol{\sigma} = \boldsymbol{\varphi} \mathbf{M}^{-T} \mathbf{z}_2$.

However, the direct method has the drawback that parameter estimates do not converge to the true values fast enough as observed in actual use [18, 20]. There are several factors causing the poor parameter estimate convergence with DARC designs: (1) A gradient type adaptation law as Eq. (63) with a constant adaptation rate matrix $\boldsymbol{\Gamma}$ that does not convergence as well as the least squares type. (2) The parameter adaptation function $\boldsymbol{\sigma}$ is driving by actual trajectory tracking error \mathbf{z}_1 , and \mathbf{z}_1 is quite small in implementation for a well designed direct adaptive control law. Thus it is more prone to be corrupted by factors such as sampling delay and noise which are neglected during synthesis of the adaptation law.

A least squares type adaptation law is used in IARC to achieve a better convergence of parameter estimates. In IARC, the adaptation rate matrix $\boldsymbol{\Gamma}$ is time-varying and

non-diagonal. The expression of standard projection mapping $\text{Proj}_{\hat{\boldsymbol{\beta}}}(\cdot)$ is

$$\text{Proj}_{\hat{\boldsymbol{\beta}}}(\cdot) = \begin{cases} \boldsymbol{\Gamma} \boldsymbol{\sigma}, \hat{\boldsymbol{\beta}} \in \bar{\Omega}_{\boldsymbol{\beta}} \text{ or } \mathbf{n}_{\hat{\boldsymbol{\beta}}}^T \boldsymbol{\Gamma} \boldsymbol{\sigma} \leq 0, \\ \left(\mathbf{I} - \boldsymbol{\Gamma} \frac{\mathbf{n}_{\hat{\boldsymbol{\beta}}} \mathbf{n}_{\hat{\boldsymbol{\beta}}}^T}{\mathbf{n}_{\hat{\boldsymbol{\beta}}}^T \boldsymbol{\Gamma} \mathbf{n}_{\hat{\boldsymbol{\beta}}}} \right) \boldsymbol{\Gamma} \boldsymbol{\sigma}, \hat{\boldsymbol{\beta}} \in \partial \Omega_{\boldsymbol{\beta}} \text{ and } \mathbf{n}_{\hat{\boldsymbol{\beta}}}^T \boldsymbol{\Gamma} \boldsymbol{\sigma} > 0, \end{cases} \quad (65)$$

where $\boldsymbol{\Gamma}(t)$ is a time-varying positive definite symmetric matrix, $\bar{\Omega}_{\boldsymbol{\beta}}$ and $\partial \Omega_{\boldsymbol{\beta}}$ is the interior and boundary of $\Omega_{\boldsymbol{\beta}}$ respectively, $\mathbf{n}_{\hat{\boldsymbol{\beta}}}$ is outward unit normal vector.

Let δ be the prediction error, the relationship between prediction error and parameter estimation error is given by

$$\delta = -\boldsymbol{\varphi}_f^T \tilde{\boldsymbol{\beta}}. \quad (66)$$

The parameter adaptation law can be described as

$$\begin{aligned} \dot{\hat{\boldsymbol{\beta}}}(t) &= \boldsymbol{\Gamma}(t) \boldsymbol{\varphi}_f(t) \delta(t), \\ \mathbf{D}_{\boldsymbol{\Gamma}} &= \mu_1(t) \boldsymbol{\Gamma}(t) - \mu_2(t) \boldsymbol{\Gamma}(t) \boldsymbol{\varphi}_f(t) \boldsymbol{\varphi}_f(t)^T \boldsymbol{\Gamma}(t), \\ \dot{\boldsymbol{\Gamma}}(t) &= \begin{cases} \mathbf{D}_{\boldsymbol{\Gamma}}, \text{ if } \lambda_M(\boldsymbol{\Gamma}(t)) < \rho_M \text{ or } \mathbf{v}_M^T \mathbf{D}_{\boldsymbol{\Gamma}} \mathbf{v}_M < 0, \\ 0, \text{ else,} \end{cases} \end{aligned} \quad (67)$$

where $\mu_1(t) \geq 0$ and μ_2 are two non-negative functions, \mathbf{v}_M is the eigenvector corresponding to $\lambda_M(\boldsymbol{\Gamma}(t))$ when $\lambda_M(\boldsymbol{\Gamma}(t)) = \rho_M$, ρ_M represents a pre-set upper bound for covariance matrix $\boldsymbol{\Gamma}(t)$.

Differentiate Eq. (56) and substitute Eqs. (59), (60) and (61) into it, then

$$\dot{\mathbf{z}}_2 = -\mathbf{K}_2 \mathbf{z}_2 + \mathbf{M}^{-1} (\mathbf{B}_c \mathbf{u}_{ds2} - \boldsymbol{\varphi}^T \tilde{\boldsymbol{\beta}}_t). \quad (68)$$

Define two positive semi-definite Lyapunov functions $V_{2a} = \mathbf{z}_2^T \mathbf{z}_2 / 2 + \tilde{\boldsymbol{\beta}}_t^T \boldsymbol{\Gamma}^{-1} \tilde{\boldsymbol{\beta}}_t / 2$ for adaptive control and $V_2 = \mathbf{z}_2^T \mathbf{z}_2 / 2$ for robust control. From Eq. (68), the time derivative of V_2 is

$$\dot{V}_2 = -\mathbf{z}_2^T \mathbf{K}_2 \mathbf{z}_2 + \mathbf{z}_2^T \mathbf{M}^{-1} (\mathbf{B}_c \mathbf{u}_{ds2} - \boldsymbol{\varphi}^T \tilde{\boldsymbol{\beta}}). \quad (69)$$

And the time derivative of V_{2a} is

$$\begin{aligned} \dot{V}_{2a} &= -\mathbf{z}_2^T \mathbf{K}_2 \mathbf{z}_2 + \mathbf{z}_2^T \mathbf{M}^{-1} \mathbf{B}_c \mathbf{u}_{ds2} \\ &\quad + \tilde{\boldsymbol{\beta}}_t^T (-\boldsymbol{\varphi}^T \mathbf{M}^{-T} \mathbf{z}_2 + \boldsymbol{\Gamma}^{-1} \dot{\tilde{\boldsymbol{\beta}}}_t). \end{aligned} \quad (70)$$

Substituting the first equation of Eq. (62) into Eq. (69),

$$\dot{V}_2 \leq -\mathbf{z}_2^T \mathbf{K}_2 \mathbf{z}_2 + \varepsilon. \quad (71)$$

Thus, \mathbf{z}_2 will exponentially converge to the ball $\mathbf{z}_2 \leq \sqrt{\varepsilon / \lambda_{\min}(\mathbf{K}_2)}$ and then be ultimately bounded. Substituting Eq. (67) and the second equation of Eq. (62) into Eq. (70), one obtains

$$\dot{V}_{2a} \leq -\mathbf{z}_2^T \mathbf{K}_2 \mathbf{z}_2. \quad (72)$$

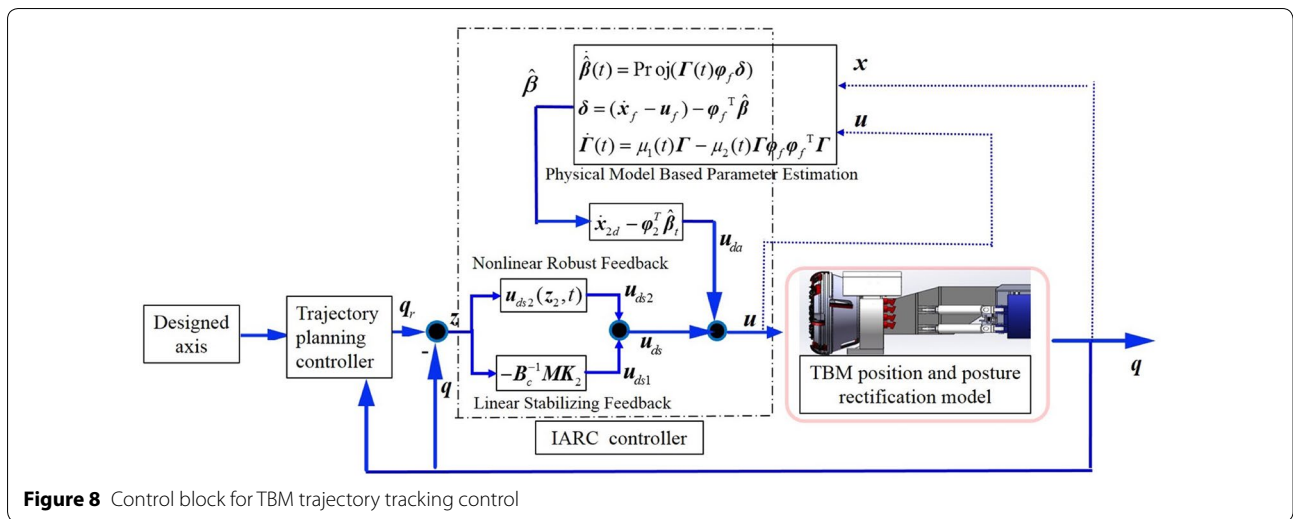


Figure 8 Control block for TBM trajectory tracking control

Hence asymptotic output tracking will be obtained.

4 Simulation Results

The control algorithms and the plant dynamics are all implemented using Matlab Simulink™ toolbox in this section. The system parameters in simulation are provided by China railway construction heavy industry Co., Ltd. The trajectory deviation ARC control strategy will be applied in TBM test-bed in China railway construction heavy industry Co., Ltd.

Figure 8 shows the proposed strategy of TBM trajectory tracking control. Compared the actual position and posture of TBM against the designed axis of tunneling construction, a planned tracking trajectory will be given by trajectory generator when the deviation oversteps the allowed scope. Then the IARC controller is designed to achieve the precise control of gripper cylinder and torque cylinders trajectory.

The accuracy of the position and posture rectification dynamic model should be checked before using the ARC controller. The hydraulic pressure of thrust cylinders are given as 1000 kN, and the hydraulic pressure of gripper cylinders and torque cylinders are set as constant values to keep the gripper carrier assembly steady. The point (10, 0, 0) is the origin of moving frame $O_Bx_By_Bz_B$ which is the centroid of shield body and main beam. The point (10, 0, 0) is treated as initial position and the X-axis direction is treated as initial orientation of TBM in this paper. Figure 9 shows the path of TBM are only in X-axis when only thrust system works in this model, which is in accord with the actual condition.

Figures 10, 11, 12, 13 show the simulation results of TBM position and posture rectification in different situations. The dotted line is the planned tracking

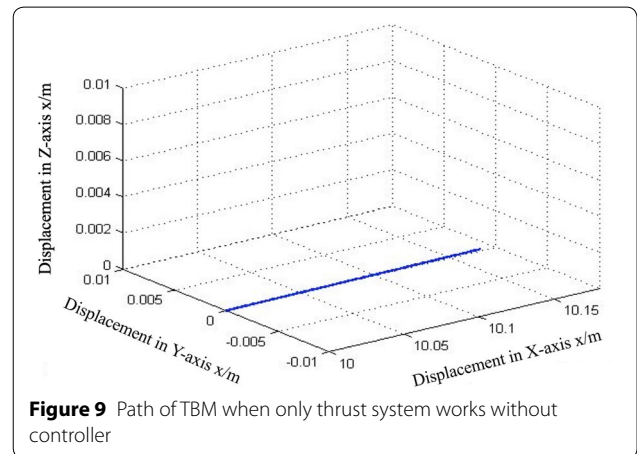


Figure 9 Path of TBM when only thrust system works without controller

trajectory, solid line represents the actual tracking trajectory and dash-dotted line is the designed trajectory of TBM construction. When the position deviation only occurs in Y-axis and the current orientation is parallel with the designed axis, the deviation can be corrected by controlling the pressure of gripper cylinder, showing in Figure 10. The actual rectification trajectory of open type TBM can track the planned tracking trajectory well under the proposed IARC controller. The actual trajectory meets the designed axis when TBM is pushed forward 0.14 m in X-axis. If the position deviation only occurs in Z-axis, then the deviation can be corrected by controlling the pressure of torque cylinders, showing in Figure 11. The initial position derivation between actual trajectory and designed axis is 0.01 m and the orientation is parallel with the designed axis. The TBM meets the designed axis when machine is pushed forward 0.145 m by thrust

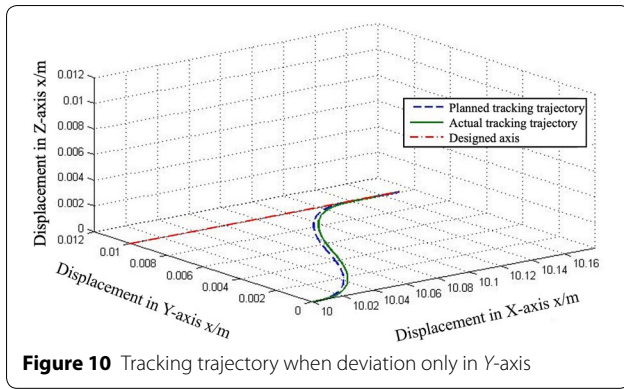


Figure 10 Tracking trajectory when deviation only in Y-axis

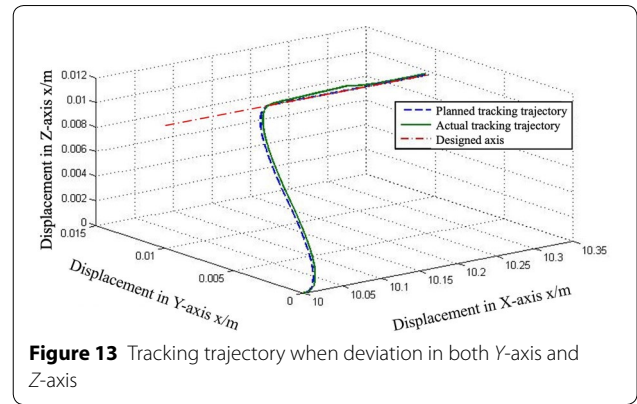


Figure 13 Tracking trajectory when deviation in both Y-axis and Z-axis

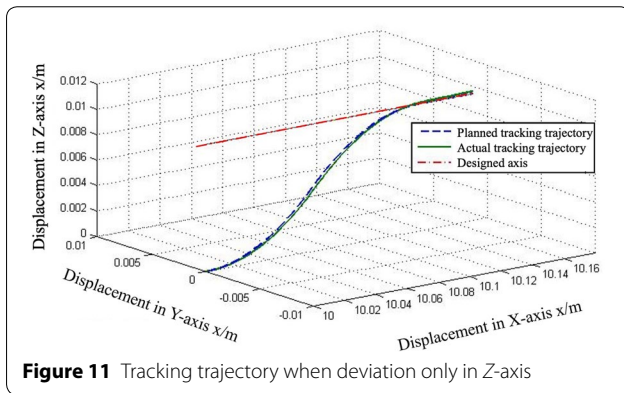


Figure 11 Tracking trajectory when deviation only in Z-axis

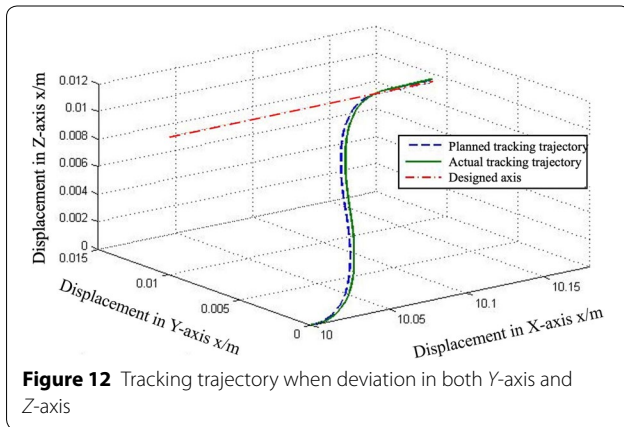


Figure 12 Tracking trajectory when deviation in both Y-axis and Z-axis

system in X-axis. If the position deviation occurs both in Y-axis and Z-axis at the same time and the current orientation is parallel with the designed axis, the pressure of gripper cylinder and torque cylinders should be controlled at the same time to rectify the deviation, which shown in Figure 12. According to the simulation results, the ARC control can track the planned tracking trajectory smoothly and rapidly. In order to validate

the performance of proposed IARC controller against the uncertain load acting on TBM, an extra load disturbance $\tau_{rd} = [0 \ 1000 \ 1000 \ 0 \ 0 \ 0]^T$ is added in the model when the TBM is pushed forward 0.15 m in X-axis. The simulation results are shown in Figure 13. The TBM actual trajectory meets the designed trajectory when TBM in X-axis is 10.28 m.

5 Conclusions

- (1) This paper mainly discusses the automatic trajectory tracking control of hard rock tunnel boring machine under complex stratum working conditions.
- (2) Mechanical structure diagram and kinematics model of gripper, torque and propel assembly has been established based on practical investigation in this paper.
- (3) An IARC controller has been put forward to achieve the precise tracking control of the planned tracking trajectory.
- (4) The results of simulation show the IARC controller can rectify the deviation smoothly and rapidly.

Authors' Contributions

ZL and HS were in charge of the whole trial; CS wrote the manuscript; JL assisted with sampling and laboratory analyses. All authors read and approved the final manuscript.

Author Details

¹ State Key Laboratory of Industrial Control Technology, Institute of Cyber-Systems and Control, Zhejiang University, Hangzhou 310027, China. ² State Key Laboratory of Fluid Power Transmission and Control, Zhejiang University, Hangzhou 310027, China.

Authors' Information

Chengjun Shao, born in 1990, is currently a PhD candidate at State Key Laboratory of Industrial Control Technology, Institute of Cyber-Systems and Control, Zhejiang University, China. He received his bachelor degree from Zhejiang University, China, in 2012. His research interests include hard rock TBM and intelligent control of shield machine.

Jianfeng Liao, born in 1991, is currently PhD candidate at *State Key Laboratory of Fluid Power Transmission and Control, Zhejiang University, China*. He received his bachelor degree from *Zhejiang University, China*, in 2013.

Zhitao Liu, born in 1982, is currently an associate professor at *State Key Laboratory of Industrial Control Technology, Institute of Cyber-Systems and Control, Zhejiang University, China*.

Hongye Su, born in 1969, is currently a professor at *State Key Laboratory of Industrial Control Technology, Institute of Cyber-Systems and Control, Zhejiang University, China*.

Competing Interests

The authors declare that they have no competing interests.

Funding

Supported by National Basic Research Program of China (973 Program, Grant No. 2013CB035406), Science Fund for Creative Research Groups of National Natural Science Foundation of China (Grant No. 61621002), and National Natural Science Foundation of China (Grant No. 61633019).

Received: 23 May 2017 Accepted: 1 April 2019

Published online: 12 April 2019

References

- [1] H Mroueh, I Shahrour. A simplified 3D model for tunnel construction using tunnel boring machines. *Tunnelling & Underground Space Technology*, 2008, 23(1): 38–45.
- [2] M Ramoni, G Anagnostou. Tunnel boring machines under squeezing conditions. *Tunnelling & Underground Space Technology*, 2010, 25(2): 139–157.
- [3] S L Shen, F X Cai, T P Li. Analysis of the internal forces in lining caused by rolling correction of DOT shield. *Chinese Journal of Geotechnical Engineering*, 2007, 29(10): 1563–1567. (in Chinese)
- [4] J H Wang. Integrated construction technology of adopting deep excavation method in shield correction. *Railway Construction Technology*, 2010, 12: 34–38. (in Chinese)
- [5] M Yue, Y Zhang. Load observer-based integral sliding mode trajectory tracking control of shield automatic tunnelling via hyperbolic tangent function. *International Journal of Modelling Identification & Control*, 2016, 25(2): 111.
- [6] M Yue, L Guo. Double closed-loop adaptive rectification control of a shield tunneling machine with hydraulic actuator dynamics subject to saturation constraint. *Journal of Vibration & Control*, 2014, 22(2): 608–614.
- [7] H B Xie, X M Duan, H Y Yang, et al. Automatic trajectory tracking control of shield tunneling machine under complex stratum working condition. *Tunnelling & Underground Space Technology*, 2012, 32(6): 87–97.
- [8] H J Liu, J C Wang, L W Zhang, et al. Dynamic modeling and trajectory tracking control of tunnel boring machine. *26th Chinese Control and Decision Conference*, Changsha, China, May 1, 2014: 4560–4565.
- [9] L Li, J F Tao, H D Yu, et al. Online condition monitoring of gripper cylinder in TBM based on EMD method. *Chinese Journal of Mechanical Engineering*, 2017, 30(6): 1325–1337.
- [10] Z H Zhang, G F Gong, Q F Gao, et al. Fragmentation energy-saving theory of full face rock tunnel boring machine disc cutters. *Chinese Journal of Mechanical Engineering*, 2017, 30(4): 913–919.
- [11] H B Xie, Z B Liu, H Y Yang. Pressure regulation for earth pressure balance control on shield tunneling machine by using adaptive robust control. *Chinese Journal of Mechanical Engineering*, 2016, 29(3): 598–606.
- [12] J Z Huo, W Z Wang, W Sun, et al. The multi-stage rock fragmentation load prediction model of tunnel boring machine cutter group based on dense core theory. *International Journal of Advanced Manufacturing Technology*, 2017, 90: 277–289.
- [13] J Z Huo, N Hou, W Sun, et al. Analyses of dynamic characteristics and structure optimization of tunnel boring machine cutter system with multi-joint surface. *Nonlinear Dynamics*, 2017, 87(1): 237–254.
- [14] J Z Huo, D Zhu, N Hou, et al. Application of a small-timescale fatigue, crack-growth model to the plane stress/strain transition in predicting the lifetime of a tunnel-boring-machine cutter head. *Engineering Failure Analysis*, 2017, 71: 11–30.
- [15] J Rostami, L Ozdemir, B Nilson. Comparison between CSM and NTH hard rock TBM performance prediction models. *Proceedings of Annual Technical Meeting of the Institute of Shaft Drilling Technology*, Las Vegas, USA, 1996: 1–10.
- [16] L Xu, B Yao. Adaptive robust precision motion control of linear motors with negligible electrical dynamics: theory and experiments. *IEEE/ASME Transactions on Mechatronics*, 2001, 6(4): 444–452.
- [17] B Yao. Integrated direct/indirect adaptive robust control of SISO nonlinear systems in semi-strict feedback form. *American Control Conference*, 2003. *Proceedings of the IEEE*, Colorado, USA, June 4–6, 2003: 3020–3025.
- [18] B Yao, F P Bu, J Reedy, et al. Adaptive robust motion control of single-rod hydraulic actuators: theory and experiments. *IEEE/ASME Transactions on Mechatronics*, 2000, 5(1): 79–91.
- [19] B Yao, M Tomizuka. Adaptive robust control of SISO nonlinear systems in a semi-strict feedback form. *Automatica*, 1997, 33(5): 893–900.
- [20] L Xu, B Yao. Observer based adaptive robust control of a class of nonlinear systems with dynamic uncertainties. *International Journal of Robust & Nonlinear Control*, 2001, 1(11): 335–356.
- [21] X C Zhu, G L Tao, B Yao, et al. Adaptive robust posture control of a parallel manipulator driven by pneumatic muscles. *Automatica*, 2008, 44(2008): 2248–2257.
- [22] K Srinivasan. Kinematic and dynamic analysis of Stewart platform-based machine tool structures. *Robotica*, 2003, 21(5): 541–554.
- [23] X Zhang, T Wang. *Computational dynamics*. Beijing: Tsinghua University Press, 2007.
- [24] B Yao. Desired compensation adaptive robust control. *The ASME International Mechanical Engineers Congress and Exposition*, California, USA, November 15–20, 1998, 64: 569–575.
- [25] B Yao, C Deboer. Energy-saving adaptive robust motion control of single-rod hydraulic cylinders with programmable valves. *American Control Conference*, Alaska, USA, May 8–10, 2002: 4819–4824.

Submit your manuscript to a SpringerOpen® journal and benefit from:

- Convenient online submission
- Rigorous peer review
- Open access: articles freely available online
- High visibility within the field
- Retaining the copyright to your article

Submit your next manuscript at ► [springeropen.com](https://www.springeropen.com)